iScience

CellPress
OPEN ACCESS

Article

Coordination of tissue homeostasis and growth by the Scribble-α-Catenin-Septate junction complex

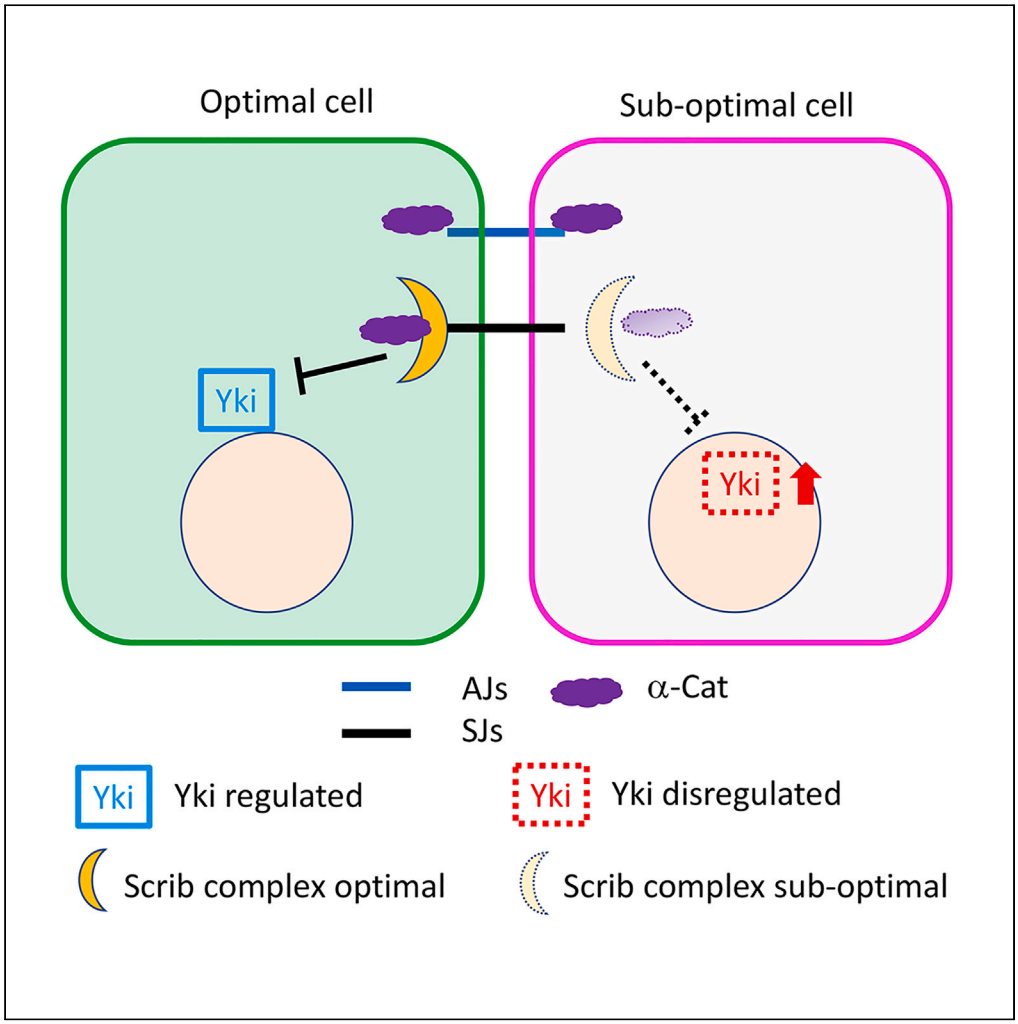

Yunxian Huang, Jinghua Gui, Satu-Marja Myllymäki, Marja L. Mikkola, Osamu Shimmi

osamu.shimmi@helsinki.fi

Highlights

Scribble interacts with α-Catenin for epithelial growth

α-Catenin-Scribble-Septate junction complex regulates Yki activity

Wildtype cells restore apicobasal polarity in *scribble* hypomorphic cells

Cellular communication contributes the robustness of polarity across the tissue

Huang et al., iScience *26*, 106490
April 21, 2023
https://doi.org/10.1016/j.isci.2023.106490

iScience

CellPress
OPEN ACCESS

Article

Coordination of tissue homeostasis and growth by the Scribble-α-Catenin-Septate junction complex

Yunxian Huang,[1,3] Jinghua Gui,[1,3] Satu-Marja Myllymäki,[1] Marja L. Mikkola,[1] and Osamu Shimmi[1,2,4,*]

SUMMARY

Maintaining apicobasal polarity (ABP) is crucial for epithelial integrity and homeostasis during tissue development. Although intracellular mechanisms underlying ABP establishment have been well studied, it remains to be addressed how the ABP coordinates tissue growth and homeostasis. By studying Scribble, a key ABP determinant, we address molecular mechanisms underlying ABP-mediated growth control in the *Drosophila* wing imaginal disc. Our data reveal that genetic and physical interactions between Scribble, Septate junction complex and α-Catenin appear to be key for sustaining ABP-mediated growth control. Cells with conditional *scribble* knockdown instigate the loss of α-Catenin, ultimately leading to the formation of neoplasia accompanying with activation of Yorkie. In contrast, cells expressing wild type *scribble* progressively restore ABP in *scribble* hypomorphic mutant cells in a non-autonomous manner. Our findings provide unique insights into cellular communication among optimal and sub-optimal cells to regulate epithelial homeostasis and growth.

INTRODUCTION

In epithelia of developing multicellular organisms, establishing apicobasal polarity (ABP) plays a key role in maintaining tissue function and homeostasis.[1,2] Epithelial cells establish distinct sub-compartments along the apicobasal axis and vectorize specific cellular functions.[3] This is achieved through the interactions or antagonisms among multiple groups of intracellular polarity determinants and intercellular junctions.[3,4]

Studies employing the *Drosophila melanogaster* wing imaginal disc, a monolayer epithelium comprising columnar cells, have greatly contributed to the understanding of ABP establishment and maintenance. In *Drosophila* epithelial cells, along the apical-to-basal axis lie multiple conserved complexes of polarity determinants: apical complex containing the Crumbs and partitioning defective (PAR) complexes, and basolateral Scribble (Scrib) complex.[3,5,6] The determinants within the same complex are interdependent as loss of either will dissociate the whole complex. On the other hand, components of distinct complexes are mutually exclusive but interactive, and thus a compromised complex failing to guard the corresponding sub-compartment will lead to either expansion or dismiss of the other complex and eventually complete loss of ABP.[4]

The Scrib module, comprising Scrib, Discs large (Dlg) and Lethal giant larvae (Lgl), localizes at lateral membranes and is enriched at septate junctions (SJs, functional counterpart of mammalian tight junctions (TJs)).[1,6,7] Loss of the Scrib module often leads to abolishment of ABP, disorganization of tissue architecture, loss of growth control and thus neoplasia.[1,8,9] This indicates that epithelial cell polarity and growth control are often tightly coupled, reflected in the fact that many molecules identified as ABP determinants serve as tumor suppressors.[1,2]

The deregulation of Scrib leads to compromised Hippo signaling pathway.[6,10,11] The Hippo pathway, a conserved regulator of organ size in animals, was identified first in *Drosophila*, where its loss results in a hippopotamus-shaped phenotype.[12,13] Hippo signaling is regulated by a variety of upstream signaling pathways including cell polarity regulation, levels of F-actin, tension within the actin cytoskeleton, and cell attachments.[12,14–17] In *Drosophila*, Yorkie (Yki), the *Drosophila* ortholog of YAP and a key effector of the Hippo pathway, is phosphorylated by Warts (wts), a homologue of Large tumor suppressor kinase 1/2 (LATS1/2) in vertebrates, to be retained in the cytoplasm or degraded, otherwise moves into the nucleus to regulate Yki-dependent transcription and growth.[12,18,19]

[1]Institute of Biotechnology, University of Helsinki, 00014 Helsinki, Finland

[2]Institute of Molecular and Cell Biology, University of Tartu, 51010 Tartu, Estonia

[3]These authors contributed equally

[4]Lead contact

*Correspondence: osamu.shimmi@helsinki.fi

https://doi.org/10.1016/j.isci.2023.106490

In epithelial morphogenesis, cell-cell communication through cellular junctions plays a crucial role in tissue development. In both *Drosophila* and mammalian epithelial cells, E-Cadherin-mediated cell-cell adhesion at adherens junctions (AJs) appear to play a central role in mediating mechanical circuit that integrates adhesion, contractile forces and biochemical signaling.[20,21] The core components of the AJs are E-Cadherin and their binding partners α-, β-, and p120-Catenins. E-Cadherin engages in adhesive complexes with neighboring cells, which are connected to the actomyosin cytoskeleton primarily via α-Catenin.[22] In contrast, the SJs in invertebrate, or TJs in vertebrate, is mainly appreciated by their role in forming the paracellular diffusion.[23,24] SJs contain ladder-like septa that span the intermembrane space.[23,25] In *Drosophila* the SJs consist of a large multi-protein complex, the parts of which are commonly utilized in vertebrate TJs, locating apically to AJs.[24,26]

In contrast with overproliferation phenotypes in the wing imaginal disc of *scrib* mutant animals, *scrib* null mutant clones are efficiently eliminated through cell competition.[27,28] This has been further investigated that suppression of Yki activity in *scrib* mutant cells is needed for cell competition.[27] Previous studies indicate that various *scrib* alleles show overproliferation phenotypes in the wing imaginal disc, but some alleles, e.g. *scrib*,[5] still appear to maintain ABP.[8,29] The Scrib N-terminal leucine rich region (LRR) domain is necessary for both cell polarity and control of cell proliferation, whereas C-terminal PDZ domains enhance the ability of the LRR to localize SJs proteins and to provide full proliferation control.[6,8] However, the detailed molecular mechanisms behind this remain to be addressed.

In this study, to understand how ABP regulates tissue growth, we investigate Scrib in the wing imaginal disc. Our findings suggest that interactions between core components of SJs, Scrib and α-Catenin appear to play a key role in ABP-mediated growth regulation. RNAi knockdown of *scrib* leads to loss of α-Catenin, resulting into neoplasia accompanying with hyperactivation of Yki. On the other hand, when *scrib* hypomorphic mutant cells are surrounded by wild type cells, ABP in mutant cells is non-autonomously restored, resulting into preservation of tissue homeostasis with restrained Yki activity. Our results thus indicate that cellular communication between optimal and sub-optimal cells leads to epithelial homeostasis and growth.

RESULTS

α-Catenin genetically and physically interacts with Scrib

Previous studies indicate that RNA interference (RNAi)-mediated knockdown (KD) of the Scrib module driven by *patched* (*ptc*)*-GAL4*, expressed in a stripe of anterior cells abutting the anterior-posterior boundary, sufficiently induced Yki dependent cell overproliferation and neoplasia in the wing imaginal disc.[10,30] To understand how ABP and growth regulation are coupled, we employed conditional knockdown of *scrib* by using temperature-sensitive GAL80 ($GAL80^{ts}$) in a combination with GAL4/UAS system (Figure 1A). Therefore, RNAi becomes functional only after temperature shift from room temperature (21°C) to 29°C. When *scrib* KD was induced at different time points, we found that initial reduction of Scrib involves the subsequent activation of Yki signal, as shown by *ex-lacZ* expression that serves as a readout of Yki activity, and increased apoptosis, followed by overproliferation that becomes evident at 4 days (4D) after temperature shift (ATS) (Figures 1B, 1C and S1A). Hyperplastic phenotypes were sufficiently suppressed (Figures 1B and1C) when wts was co-expressed in *scrib* KD cells, consistent with previous studies that ectopic Yki activity is key for overproliferation after *scrib* KD.[10] Importantly, ectopic expression of constitutive active Yki (caYki) or knockdown of *wts* (*wts* RNAi) is not sufficient for neoplasia formation (Figure S1B). Notably, with *wt* expression, *scrib*-KD cells remain integrated within the wing epithelia (Figure 1B), suggesting that additional components are involved in hyperactivation of Yki in ABP-compromised cells.

Cell-cell communication of epithelial cells is often mediated through AJs.[31] To address the molecular mechanisms underlying ABP-mediated growth control, we first tested how key components of AJs are affected after conditional *scrib* KD (2D ATS). Our data reveal that DE-Cadherin (DE-Cad) and β-Catenin (β-Cat) remain intact, although their expression is significantly decreased after *DE-cad* KD (Figures 1D, 1E and S1C). In contrast, α-Catenin (α-Cat) expression significantly decreased in either *scrib* or *DE-cad* KD (Figures 1D and1E). α-Cat was synergistically depleted when *scrib* and *DE-cad* were simultaneously knocked down (dKD; Figures 1D and1E). Loss of α-Cat caused by *scrib* RNAi appears to occur in a post-transcriptional manner because *α-Cat* mRNAi level is not reduced in the Ptc domain (Figure S1D). We also confirmed that α-Cat biochemically interacts with LRR domains and PDZ3/4 domains of Scrib (Figures S1E and S1F). These results suggest that α-Cat may be a thus far insufficiently characterized factor involved in the regulation of the Scrib complex.

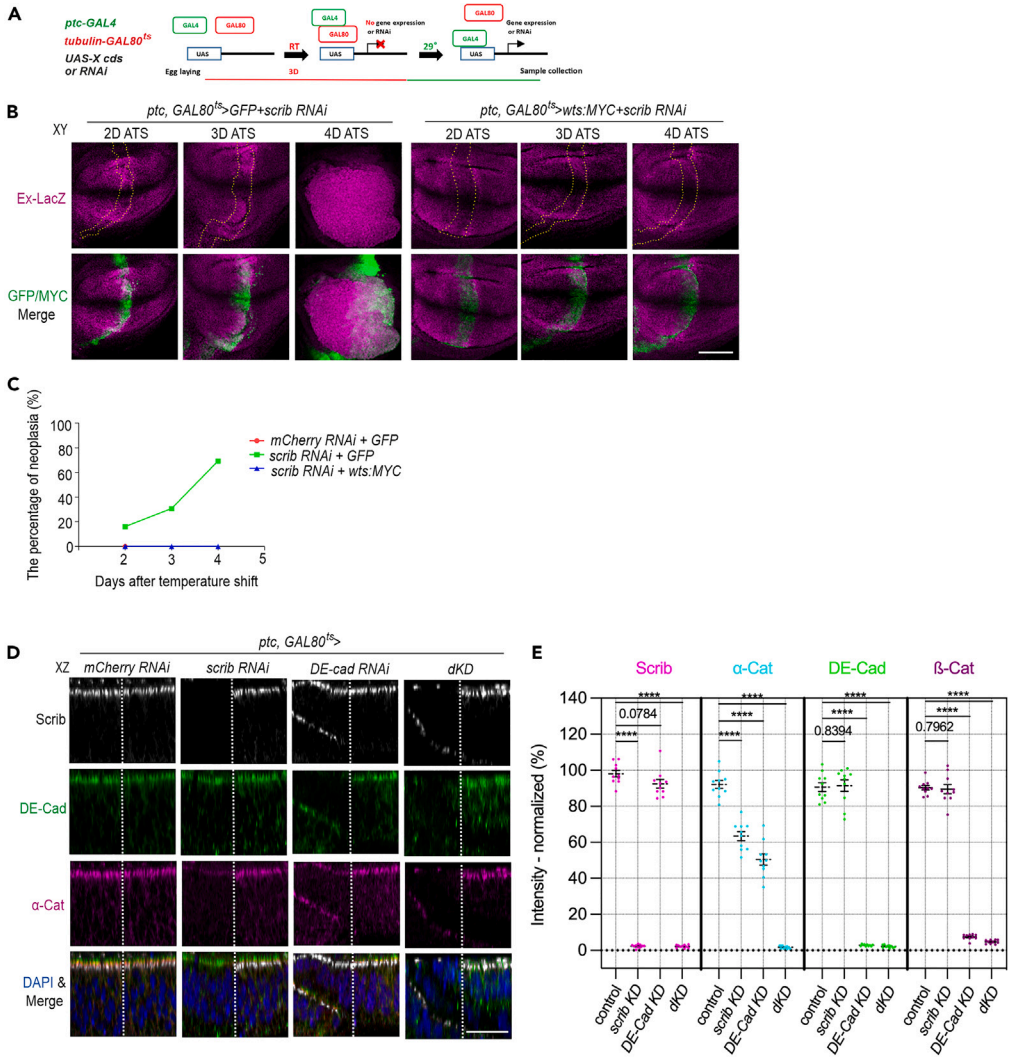

Figure 1. α-Catenin associates with Scrib

(A) Schematic of conditional RNAi knockdown by using GAL80^{ts} together with the GAL4/UAS system.

(B) Representative coronal (XY) images showing the wing pouch with conditional expression of *GFP* and *scrib RNAi*, or *wts:MYC* and *scrib RNAi* driven by *ptc-GAL4*. Tissues were collected between 2 and 4 days after temperature shift (ATS) for immunofluorescent analyses, labeled with *ex-lacZ* (magenta), and GFP or MYC (Green). The dash lines outline GFP/MYC-positive cells.

(C) Quantification of the percentage of the neoplasia. Sample sizes are 48 (*mCherry* RNAi 2D ATS), 74, 78 and 68 (*scrib* RNAi 2D, 3D and 4D ATS), and 54, 58 and 54 (*scrib* RNAi and *wt:MYC* 2D, 3D and 4D ATS).

(D) Representative transverse section (XZ) images showing the wing imaginal disc with conditional expression of *mCherry* RNAi alone (control), *scrib* RNAi (*scrib* KD), *DE-cad RNAi* (*DE-cad* KD) or *scrib*/*DE-cad RNAi* (dKD) driven by *ptc-GAL4*. Tissues were collected two days after temperature shift (ATS) for immunofluorescent analyses, labeled with Scrib (gray), DE-Cad (green), α-Cat (magenta) and DAPI (blue). The dash lines outline the anterior-posterior boundary. Anterior is to the left. Anterior domain in the figure corresponds to the *ptc* expression.

(E) Fluorescent intensity measurements of Scrib, α-Cat, DE-Cad and β-Cat in the *ptc* expression area with RNAi, normalized to that of the abutting posterior area. Sample sizes are 10 in each quantification. ****p< 0.0001. Data are means ±95% confidence intervals (CIs). Statistical significance was calculated by the two-tailed *t*-test. Scale bars, 50 μm (B), and 20 μm (D). See also Figure S1.

Association of α-Catenin with Scrib facilitates cortical localization of Scrib

How is α-Cat involved in Scrib signaling? Previous studies suggest that Scrib-LRR domains are indispensable for ABP establishment, whereas Scrib-PDZ domains support it by stabilizing cortical Scrib.[8] We

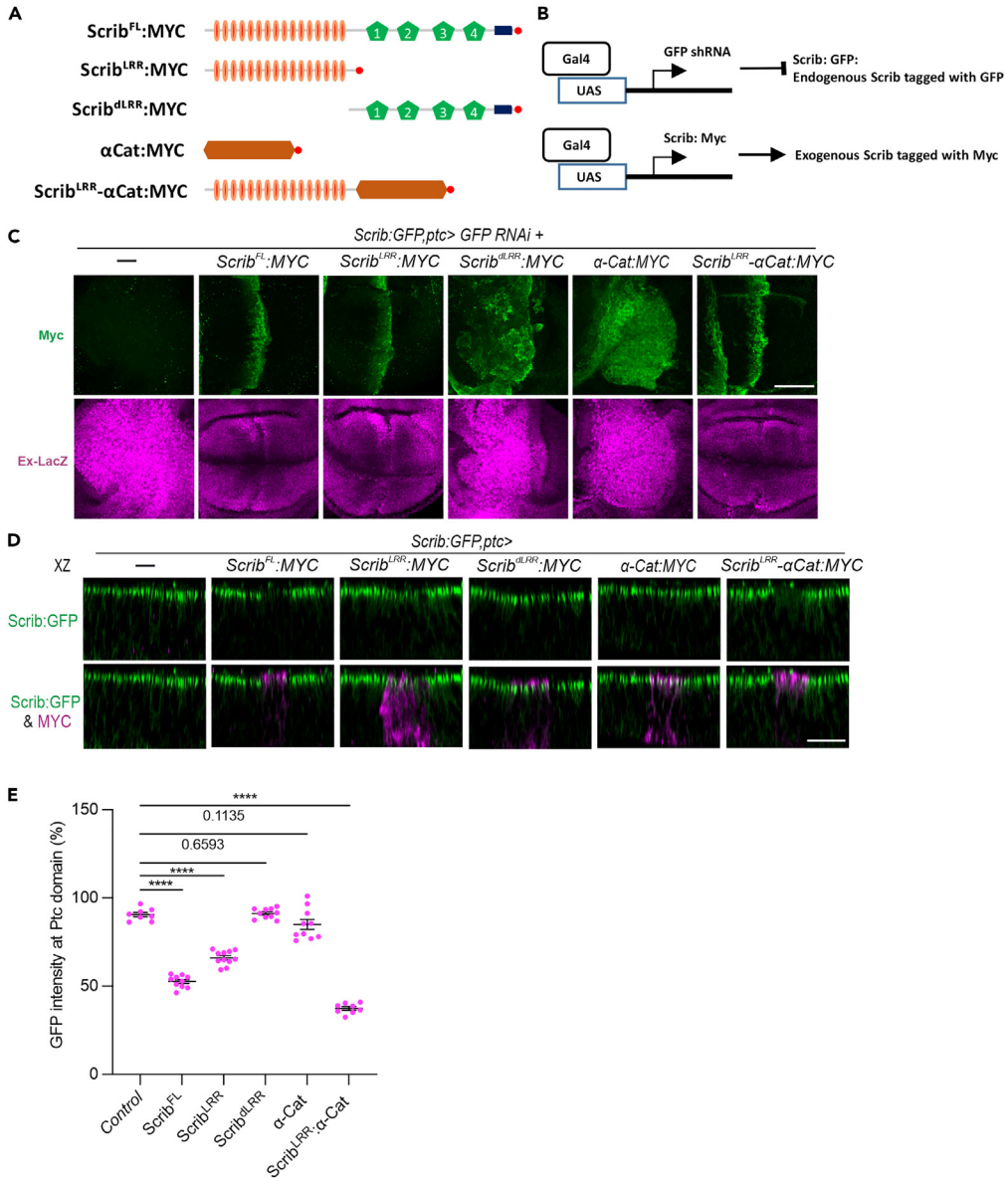

Figure 2. α-Catenin facilitates cortical localization of Scrib

(A) Schematics show the fragments of Scrib used in the functional rescue of *scrib* KD cells and the immunostaining.

(B) Schematics show *scrib KD* by *gfp* RNAi and co-expression of the fragments of Scrib.

(C) Representative coronal (XY) images showing the wing pouch with expression of *gfp* RNAi and $Scrib^{FL}$, $Scrib^{LRR}$, $Scrib^{dLRR}$, *α-Cat*, or $Scrib^{LRR}$:*α-Cat* driven by *ptc-GAL4* in GFP-trapped Scrib (Scrib:GFP) animals. Tissues were collected for immunofluorescent analyses, labeled with MYC (green) and ex-lacZ (magenta).

(D) Representative transverse section (XZ) images showing the wings with expression of $Scrib^{FL}$, $Scrib^{LRR}$, $Scrib^{dLRR}$, *α-Cat, or* $Scrib^{LRR}$:*α-Cat* driven by *ptc-GAL4* in Scrib:GFP animals. Tissues were collected for immunofluorescent analyses, labeled with Scrib:GFP (green) and MYC (magenta).

(E) Quantification of relative Scrib:GFP intensity in (D) at the Ptc expressing domain. Sample sizes are 8 (control), 10 ($Scrib^{FL}$), 11 ($Scrib^{LRR}$), 10 ($Scrib^{dLRR}$) 10 (α-Cat) and 8 ($Scrib^{LRR}$:α-Cat). ****p< 0.0001. Data are means ±95% confidence intervals (CIs). Statistical significance was calculated by the two-tailed *t*-test. Scale bars, 50 μm (C), and 20 μm (D).

therefore hypothesize that α-Cat may help stabilize Scrib localization at the cortical domain through interaction with PDZ domains. To test this hypothesis, we generated and expressed various constructs in the wing imaginal disc to compensate loss of *scrib* (Figures 2A and 2B). By employing fully functional GFP trapped Scrib (Scrib:GFP) as a host line,[32] Scrib:GFP was knocked down by *gfp* RNAi in the Ptc domain.

Hyperactivation of Yki signal (ex-lacZ) was observed across the tissue (Figure 2C), which mimics *scrib* KD phenotype (Figure S1B), indicating that *gfp* RNAi efficiently knocked down *scrib*. When various constructs were co-expressed, $Scrib^{FL}$ or $Scrib^{LRR}$ sufficiently restored *scrib* KD phenotypes (Figure 2C). Although restoration was not observed by co-expression of either $Scrib^{dLRR}$ or α-Cat, $Scrib^{LRR}$:α-Cat chimera protein significantly rescued tissue malformation and ectopic Yki activity within the wing pouch (Figure 2C).

Next cellular distributions of various constructs were investigated. When MYC-tagged $Scrib^{FL}$ proteins were overexpressed in Scrib:GFP flies, we observed that $Scrib^{FL}$:MYC becomes more dominantly localized at the cortical domain where Scrib:GFP is located (Figures 2D and 2E). Of interest, $Scrib^{LRR}$:α-Cat:MYC chimera recapitulates the pattern of $Scrib^{FL}$ and outcompetes Scrib:GFP (Figures 2D and 2E). In contrast, while $Scrib^{LRR}$:MYC affects Scrib:GFP but also shows broader distribution at the cell periphery (Figures 2D and 2E). Nevertheless, α-Cat alone (α-Cat:MYC) or $Scrib^{dLRR}$:MYC barely affects Scrib:GFP (Figures 2D and 2E). Taken together these data suggest that the association of α-Cat facilitates cortical localization of Scrib, although Scrib-LRR domains sufficiently restore *scrib* KD phenotypes when they are surrounded by wild type cells.

A genetic interaction between α-Catenin and septate junction components contributes to Scrib mediated growth control

Given that Scrib complex is enriched around and functions as co-factor of SJs,[24,33] we wondered whether core-components of SJs, Scrib complex and α-Cat mutually interact to sustain ABP-mediated growth control. To corroborate this, we examined how Scrib distribution is affected by depleting α-Cat and SJs components. Conditional KD of *α-Cat* alone reveals that Scrib distribution was barely affected by 2D ATS (Figure S3A), and could not be investigated further because of cell death and tissue malformation from 3D ATS onwards. In contrast, conditional double KD (dKD) of *α-Cat* and SJs components (*NrxIV* or *Kune*) leads to reduced expression of Scrib in a part of cells abutting the anterior-posterior boundary by 2D ATS (Figure S3A). The results are further confirmed by alternative approach. We employed *nubbin (nub)-GAL4* whose activity is across the whole wing pouch to perform the KD experiments. Of interest, *α-Cat* KD gave rise to patchy loss of Scrib whereas most cells seem unaffected (Figure S3B). However, on dKD, a vast majority of cells within the wing pouch were devoid of Scrib (FigureS3B). These data suggest that α-Cat can genetically interact with SJs components to regulate Scrib localization. Altogether, these results clearly indicate the genetic interactions between α-Cat, Scrib and core-components of SJs.

Next, we hypothesized that α-Cat interacting with SJs complex may play a role in sustaining Scrib function. To test this, we generated multiple constructs to compensate loss of *scrib* (Figure 3A). By using GFP trapped line Scrib:GFP *scrib* KD phenotypes were observed by *gfp* RNAi (Figure 2C). Although restoration of *scrib* KD phenotypes was not observed when either α-Cat or Kune was co-expressed (Figures 2C and 3B), Kune:α-Cat chimera protein significantly rescued tissue malformation and ectopic Yki activity within the wing pouch (Figure 3B). We then further investigated how ABP and tissue homeostasis are regulated by combining conditional *scrib* KD and ectopic expression of chimera proteins. Our data reveal that co-expression of the Kune:α-Cat chimera significantly suppressed neoplasia formation from the conditional *scrib* KD (Figures 3C and 3D). Importantly, such restoration phenotypes were not observed when DE-Cad:α-Cat chimera was expressed (Figures 3B–3D). We next studied subcellular localization of Kune:α-Cat chimera protein. When subcellular localization of DE-Cad and SJs component NrxIV were visualized in the wing imaginal disc, DE-Cad and NrxIV show continuous but distinct distributions, indicating the positions of AJs and SJs, respectively (Figure S3C). When α-Cat alone was expressed, α-Cat was largely overlapped with DE-Cad and a small fraction of α-Cat was localized with NrxIV (Figure S3C). In contrast, Kune was localized at basal part of DE-Cad and apical part of NrxIV and weakly distributed in a broader area (Figure S3C). Of interest, Kune:α-Cat chimera was localized at basal part of DE-Cad and apical part of NrxIV (Figure S3C). Taken together, these results suggest that α-Cat localized with SJs components through Scrib regulates Yki activity, therefore contributing to maintain tissue homeostasis.

The dosage of Scrib affects apicobasal polarity-mediated growth control

We next address how the quantity of Scrib complex plays a role in ABP-mediated growth control. To understand this, we knocked down *scrib* in flies expressing *scrib* at various levels. When these experiments were tested in flies with one null allele of *scrib* ($scrib^2$/+), which develops normally, tissue disorganization and neoplasia were frequently observed by 3D ATS (Figures 4A–4C). The haploinsufficiency of *scrib* that is not detectable during homeostasis is manifested when $scrib^2$/+ cells are facing the ABP-compromised

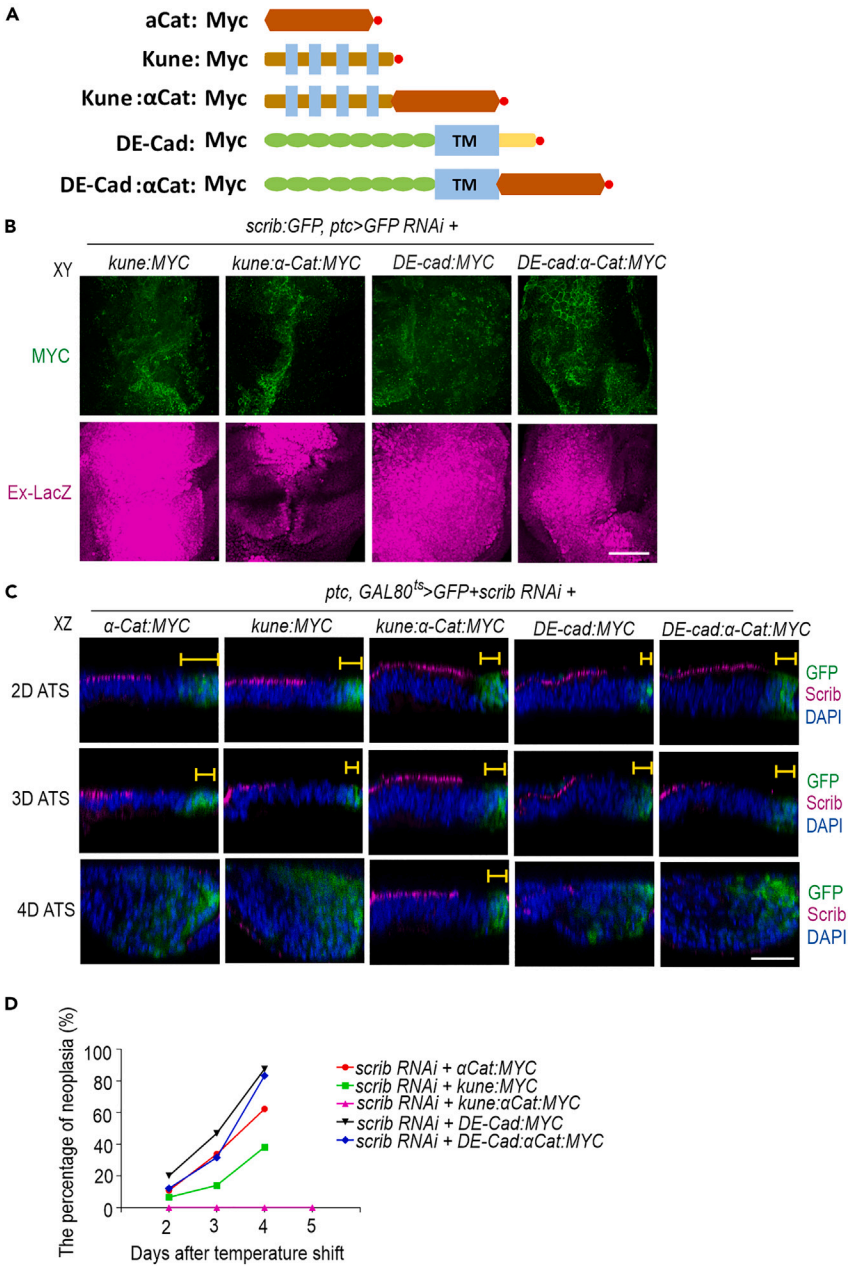

Figure 3. α-Catenin associates with SJs to sustain apicobasal polarity-mediated growth

(A) Schematics show the constructs used in the functional rescue of *scrib* KD cells.

(B) Representative coronal (XY) images showing the wing pouch with expression of *gfp* RNAi and *kune*, *kune:α-Cat*, *DE-cad*, or *DE-cad:α-Cat* driven by *ptc-GAL4* in GFP-trapped Scrib (Scrib:GFP) animals. Tissues were collected for immunofluorescent analyses, labeled with MYC (green) and ex-lacZ (magenta).

(C) Representative transverse section (XZ) images showing the wings with conditional expression of *GFP* and *scrib RNAi* together with *α-Cat*, *kune*, *kune:α-Cat*, *DE-cad* or *DE-cad:α-Cat* driven by *ptc-GAL4*. Tissues were collected at 2–4 days after temperature shift (ATS) for immunofluorescent analyses, labeled with Scrib (magenta), GFP (green) and DAPI (blue). The brackets indicate the apical range of GFP-positive cells.

(D) Quantification of the percentage of the neoplasia. Sample sizes are 74, 71 and 61 (*scrib* RNAi and *α-Cat:MYC* 2D, 3D and 4D ATS), 62, 43 and 55 (*scrib* RNAi and *kune:MYC* 2D, 3D and 4D ATS), 63, 54, 79 and 67 (*scrib* RNAi and *kune:α-Cat:MYC* 2D, 3D 4D and 5D ATS), 40, 64 and 64 (*scrib* RNAi and *DE-cad:MYC* 2D, 3D and 4D ATS), and 58, 38 and 54 (*scrib* RNAi and *DE-cad:α-Cat:MYC* 2D, 3D and 4D ATS). Scale bars, 50 μm (B) and 30 μm (C). See also Figure S3.

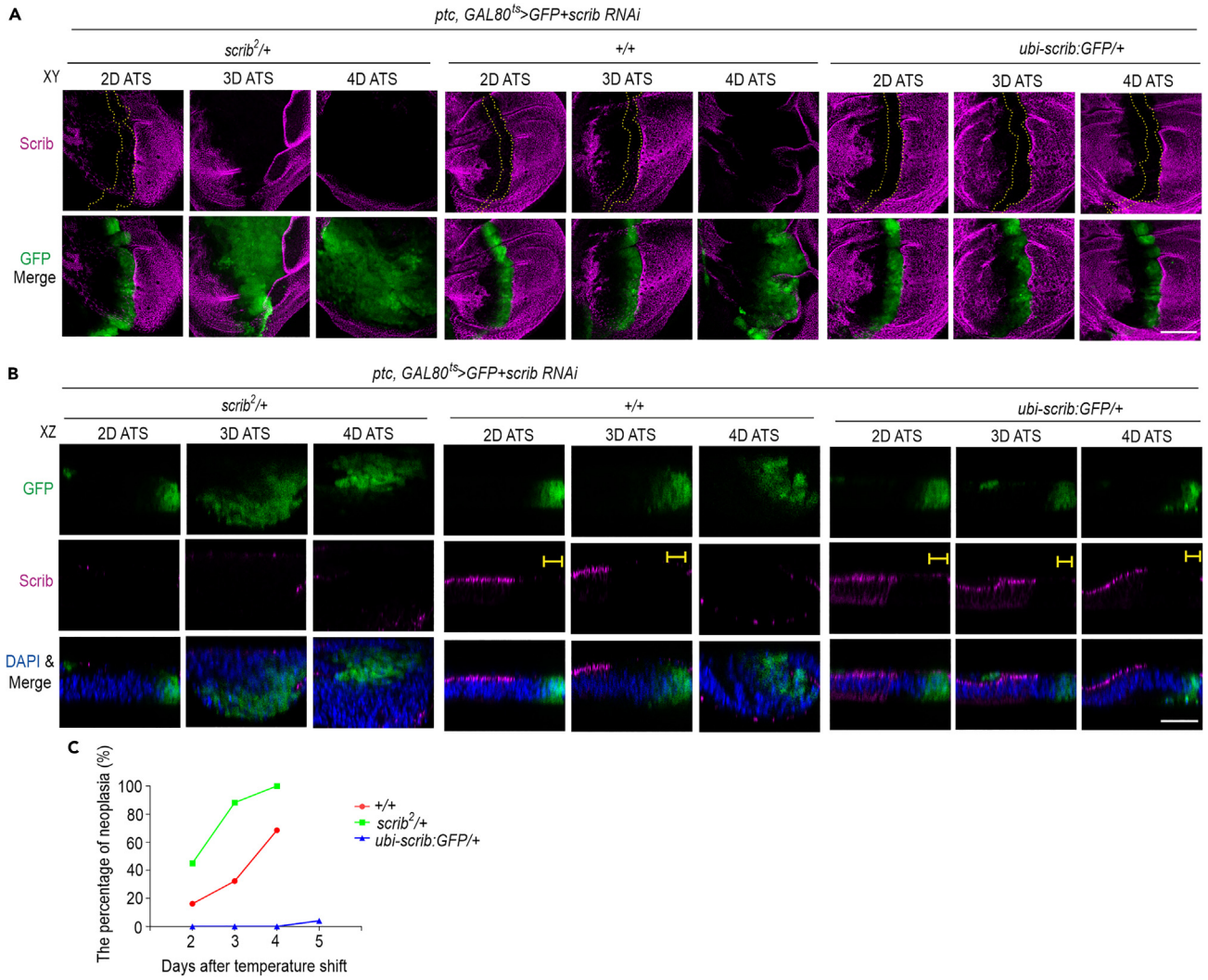

Figure 4. The dosage of Scrib affects apicobasal polarity mediated growth control

(A and B) Representative coronal (XY, A) or transverse section (XZ, B) images showing the wing pouch with conditional expression of *GFP* and *scrib RNAi* driven by *ptc-GAL4* in *scrib*^{2}/+, +/+ or *ubi-scrib*/+animals. Tissues were collected between 2 and 4 days after temperature shift (ATS) for immunofluorescent analyses, labeled with Scrib (magenta), GFP (green) and DAPI (blue). The dash lines outline GFP-positive cells (A). The brackets indicate the apical range of GFP-positive cells (B).

(C) Quantification of the percentage of the neoplasia. Sample sizes are 56, 62 and 54 (*scrib* RNAi in +/+ 2D, 3D and 4D ATS), 40, 85 and 63 (*scrib* RNAi in *scrib*^{2}/+ 2D, 3D and 4D ATS), and 42, 35, 38 and 50 (*scrib* RNAi in *ubi-scrib*/+2D, 3D 4D and 5D ATS). Scale bars, 50 μm (A), 30 μm (B).

cells, suggesting amount of Scrib protein is important to maintain robustness of wing disc development. To validate this further, we used tissue with ectopic Scrib by expressing exogenous Scrib under the control of the polyubiquitin promoter (*ubi-scrib*). Of interest, even though ABP loss in the cells abutting *scrib* KD cells still occurs by 2D ATS, tissue disorganization and neoplasia were sufficiently suppressed even by 5D ATS (Figures 4A–4C). These results reveal that the loss of function of *scrib* differentially impact on tissue architecture and overall the growth within the tissue with different dosages of *scrib*.

Scrib^{5} contributes to apicobasal polarity in wing epithelial cells in a context-dependent manner

In contrast to elimination of *scrib* null mutant clones in the wing imaginal disc through cell competition,[27-] *scrib* knockdown, a partial loss-of-function of *scrib*, cells generate neoplasia.[10,30] We then wondered what happens when *scrib* hypomorphic mutant clones are generated. Previous studies indicate that a hypomorphic *scrib* allele, *scrib*,^{5} shows overproliferation phenotypes in the wing imaginal disc but appears to

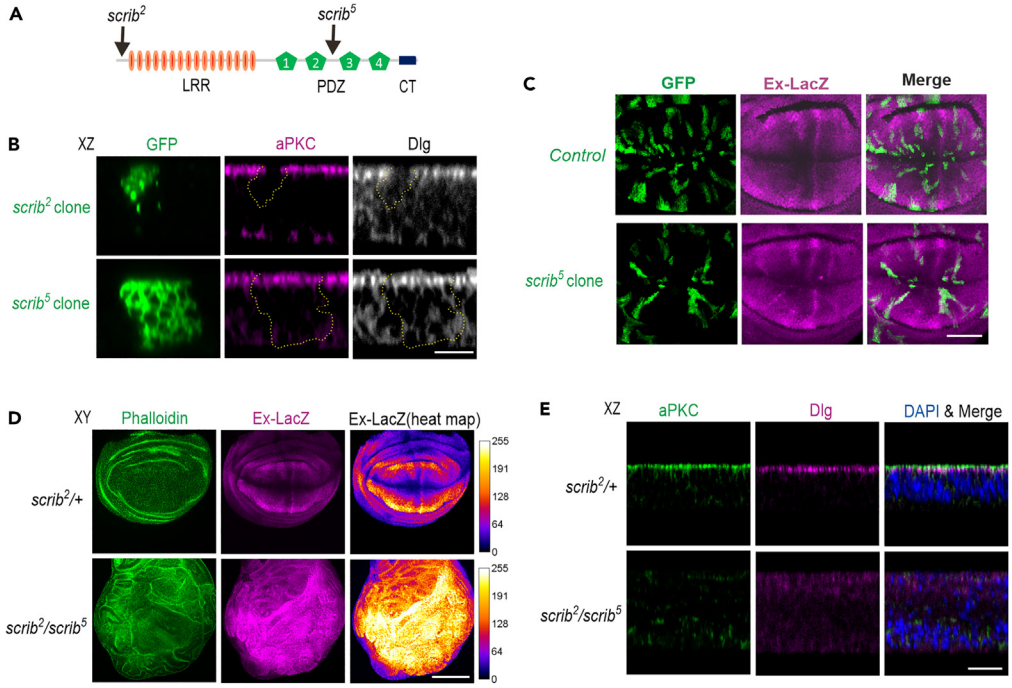

Figure 5. Intercellular restoration of apicobasal polarity in wing epithelial cells

(A) A schematic showing the secondary structure of Scrib, and the position where premature stop codons are found in *scrib*^{2} and *scrib*^{5} mutations. Approximate positions of leucine rich region (LRR), Psd95-Dlg-Zo1 (PDZ) and C-terminal (CT) domains are labeled.

(B) Representative transverse section (XZ) images showing mosaic studies of *scrib*^{2} or *scrib*^{5}mutant cells labeled with mCD8:GFP (green); the tissues were co-stained with aPKC (apical marker, magenta) and Dlg (basolateral marker, gray). Apical is up and basal bottom.

(C) MARCM analysis of control and *scrib*^{5} clones (GFP positive, green). Tissues were co-stained with *ex-lacZ* (magenta).

(D) Representative coronal (XY) images showing the wing pouch of *scrib*^{2}/+or *scrib*^{2}/*scrib*^{5}mutant animals, labeled with phalloidin (F-Actin, green) and ex-lacZ (Yki activity, magenta). Dorsal is up and ventral bottom. Anterior is left and posterior right. Heatmap showing the intensities of LacZ staining. A scale for the heat maps is indicated on the right. The heatmap was produced using the ROI color coder plugin, matching measurements to a color of a lookup table (LUT) of ImageJ/FIJI.

(E) Representative transverse section (XZ) images showing the wing pouch of *scrib*^{2}/+or *scrib*^{2}/*scrib*^{5}mutant animals, labeled with aPKC (green), Dlg (magenta) and merged with DAPI (nuclear marker, blue). Scale bars, 10 μm (B), 50 μm (C), 100 μm (D) and 20 μm (E). See also Figure S5.

maintain ABP, indicating that the N-terminal LRR domain might be sufficient for ABP, but not growth control.[8,29] To investigate this further, we employed mosaic analysis with a repressible cell marker (MARCM), using two distinct *scrib* mutant alleles in the *Drosophila* wing imaginal disc (Figure 5A).[34] When null mutant clones (*scrib*^{2}) were introduced, only very small-size clones were produced and accompanied by an autonomous reduction of expression of atypical protein kinase C (aPKC), an apical marker, and Dlg (Figure 5B).[27,28] To understand how Scrib distributions are regulated within and outside of the *scrib*^{2}mutant clones, we generated larger *scrib*^{2}mutant clones expressing dominant-negative form of *Drosophila* JNK Basket (Bsk^{DN}).[27] Loss of Scrib staining is observed within the *scrib*^{2}mutant clones (Figure S5). In contrast, clones of *scrib,*^{5} which contains a stop codon between second and third PDZ domains, do not show significant changes of aPKC and Dlg spatial distribution (Figures 5A and 5B). Furthermore, when *scrib*^{5} clones were generated, change of Yki activity in the clone cells are rather limited (Figure 5C). These results suggest that Scrib^{5} protein is sufficient for maintaining ABP in wing epithelial cells when *scrib*^{5} cells are surrounded by wild type cells. In contrast, the wing discs from *scrib*^{5} (*scrib*^{2}/*scrib*^{5}) animals show overproliferation phenotypes accompanied by significant activation of Yki (Figure 5D).[35] Our data also showed that distinct compartments of aPKC and Dlg dissipated (Figure 5E), indicating that ABP is not properly maintained in *scrib*^{5} tissues, and accordingly growth control appears to be defective. This suggests that *scrib*^{5} cells *per se* are incompetent in maintaining ABP and primed for malignancy.

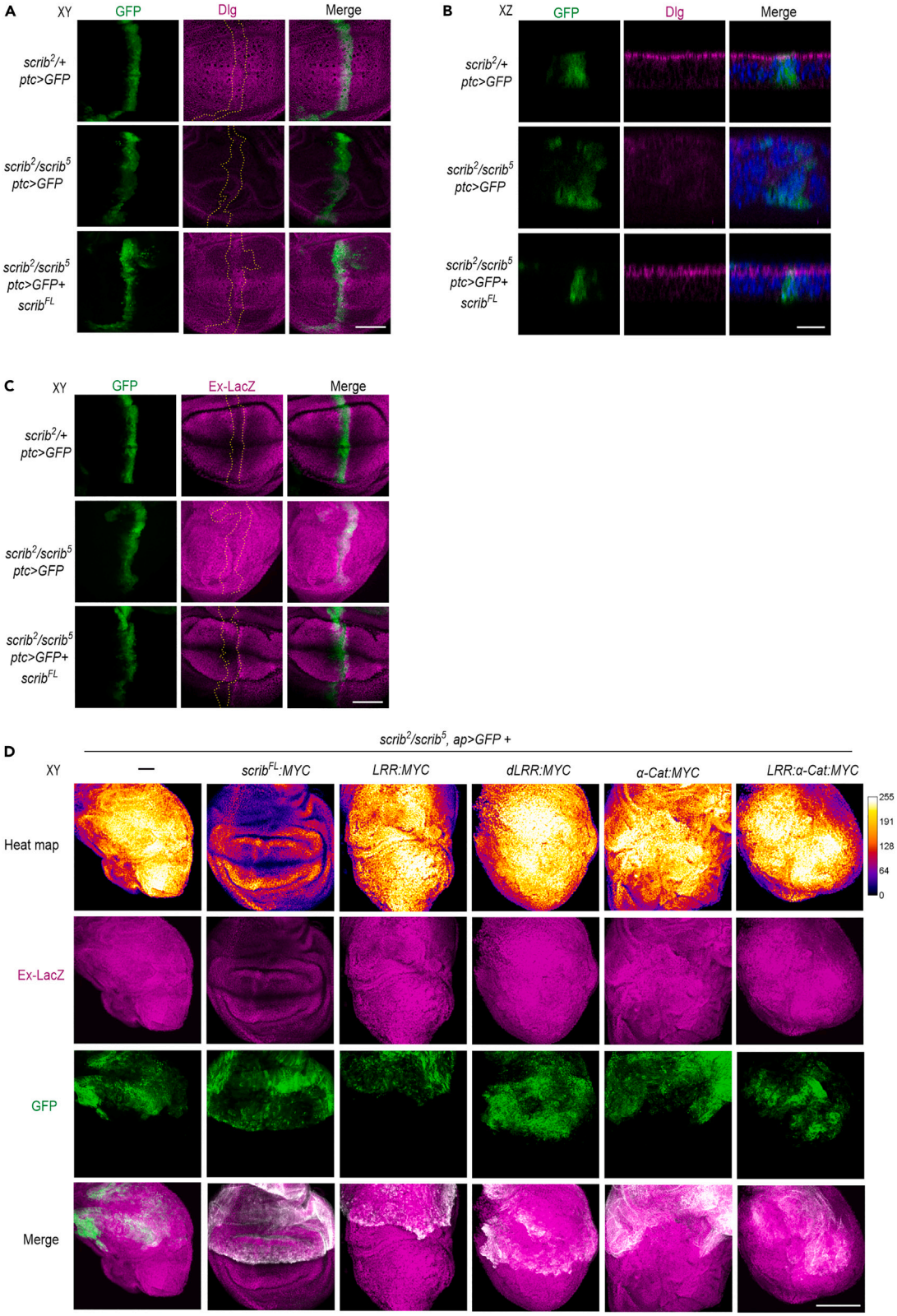
A
XY
GFP
Dlg
Merge
scrib2/+ ptc>GFP
scrib2/scrib5 ptc>GFP
scrib2/scrib5 ptc>GFP+ scribFL
B
XZ
GFP
Dlg
Merge
scrib2/+ ptc>GFP
scrib2/scrib5 ptc>GFP
scrib2/scrib5 ptc>GFP+ scribFL
C
XY
GFP
Ex-LacZ
Merge
scrib2/+ ptc>GFP
scrib2/scrib5 ptc>GFP
scrib2/scrib5 ptc>GFP+ scribFL
D
scrib2/scrib5, ap>GFP +
XY
—
scribFL:MYC
LRR:MYC
dLRR:MYC
α-Cat:MYC
LRR:α-Cat:MYC
Heat map
Ex-LacZ
GFP
Merge
255
191
128
64
0

Figure 6. Scrib and apicobasal polarity in wing epithelial cells

(A and B) Representative coronal (XY, A) or transverse section (XZ, B) images showing the wing pouch of *scrib*^{2}/+or *scrib*^{2}/*scrib*^{5}mutant animals expressing GFP alone or GFP (green) and *scrib*^{FL} driven by *ptc-GAL4* driver. Tissues were co-stained with Dlg (magenta) and DAPI (blue). Numbers of neoplastic wing imaginal discs have been seen in 0 out of 24 in *scrib*^{2}/+, *ptc>GFP*; 28 out of 32 in *scrib*^{2}/*scrib*^{5}, *ptc>GFP*; 5 out of 34 in *scrib*^{2}/*scrib*^{5}, *ptc>GFP + scrib*^{FL}.

(C) Representative coronal (XY) images showing the wing pouch of *scrib*^{2}/+ or *scrib*^{2}/*scrib*^{5} mutant animals expressing GFP alone, or GFP and *scrib*^{FL} driven by *ptc-GAL4* driver. Tissues were co-stained with ex-lacZ (magenta).

(D) Representative coronal (XY) images showing the wings expressing *GFP* with *Scrib*^{FL}, *Scrib*^{LRR}, *Scrib*^{dLRR}, *α-Cat*, *or Scrib*^{LRR}:*α-Cat* driven by *ap-GAL4* in the background of *scrib*^{2}/*scrib*^{5}, labeled with ex-lacZ (magenta) and GFP. Heatmap showing the intensities of LacZ staining. A scale for the heat maps is indicated on the right. The dashed lines outline GFP-positive cells (A, C). Scale bars, 50 μm (A, C), 20 μm (B) and 100 μm (D). See also Figure S6.

Intercellular restoration of apicobasal polarity is regulated to maintain homeostasis of *scrib*^{5} cells

Given that *scrib*^{5} clone cells maintain ABP, we wondered whether ABP in *scrib*^{2}/*scrib*^{5} tissues might be restored when full length *scrib* (*scrib*^{FL}) is expressed in neighboring cells. To test this, Scrib^{FL} was expressed by *ptc-GAL4* in the *scrib*^{2}/*scrib*^{5} wing imaginal disc. Remarkably, tissue architecture was thoroughly restored, and Dlg distribution was largely normal across the tissue (Figures 6A and 6B). Yki signal was also restored in the entire tissue (Figure 6C). We then addressed whether various constructs restore tissue architecture and Yki signal in the *scrib*^{2}/*scrib*^{5} wing imaginal discs. By employing the system that induce ectopic expression in the dorsal compartment (driven by *apterous (ap)-GAL4*) of *scrib*^{2}/*scrib*^{5} wing imaginal discs, we confirmed that Scrib^{FL} sufficiently restored mutant phenotypes in both dorsal and ventral cells (Figures 6D, S6A and S6B). In contrast, none of the Scrib fragments including Scrib^{LRR}:α-Cat chimera could restore *scrib*^{2}/*scrib*^{5} phenotypes (Figures 6D, S6A and S6B). Importantly, ectopic expression of *wts* in the dorsal compartment could not restore mutant phenotype as well (Figure S6B), suggesting that suppressing Yki signal is not sufficient for restoring ABP. Taken together, these results reveal that cells expressing *scrib*^{FL} non-autonomously restore ABP in *scrib*^{2}/*scrib*^{5} cells, resulting into regulating tissue homeostasis.

DISCUSSION

Here, our studies employing conditional RNAi KD show that α-Cat plays a key role in sustaining ABP-mediated growth control in the *Drosophila* wing imaginal disc. In addition to previously proposed α-Cat function at AJs,[22] our findings reveal that α-Cat appears to be also functional at SJs as follows. First, cellular localization of α-Cat is partly regulated by Scrib (Figure 1). Second, α-Cat biochemically interacts with Scrib (Figure S1). Third, double knockdown of α-Cat and core component of SJs affect Scrib distribution (Figure S3). Fourth, chimera proteins of α-Cat with Scrib^{LRR} domain facilitate cortical localization around SJs (Figure 2). Fifth, Kune:α-Cat chimera expression in *scrib* KD cells significantly suppresses hyperactivation of Yki activity and neoplasia formation (Figure 3). Because α-Cat, as a scaffold protein, displays multiple interactions and functions together with other proteins, loss of function of *α-Cat* does not show clear cut ABP phenotypes.[22] Nevertheless, our data sufficiently support that α-Cat is involved in the Scrib-SJs pathway for tissue growth and homeostasis in the wing imaginal disc. Moreover, α-Cat-Scrib interaction regulating Yki/YAP signal appear to be evolutionarily conserved between vertebrates and invertebrates in epithelial cells.[36] Furthermore, this process is significantly affected by dosage of Scrib, resulting into differential neoplasia formation (Figure 4), suggesting the active engagement of α-Cat-Scrib-SJs pathway in physiological and pathological conditions.

In the case of *scrib*^{5} mutants, tissue homeostasis is safeguarded by intercellular restoration of ABP. Cellular communication between optimal and sub-optimal cells has been previously investigated, demonstrating that cell competition plays a crucial role in tissue homeostasis.[28,37,38] In contrast to the competition paradigm, in which sub-optimal/loser cells are eliminated to maintain tissue homeostasis or restrain hyperplasia, our studies show that intercellular restoration of ABP serves as an additional pathway that coordinates integration of cells through intercellular ABP regulation. We postulate that intercellular restoration of ABP requires "seeds" in recipient cells, because our data reveal that a mildly truncated form of Scrib appears to be needed for ABP restoration. In contrast, *scrib*^{2} cells cannot establish ABP because of their lacking minimal Scrib protein elements, most likely LRR domain of Scrib, and are subject to elimination through cell competition.[27,28] Although precise molecular mechanisms behind intercellular restoration of ABP remain to be addressed, ABP restoration offers a distinct model for studying tissue homeostasis.

Because expression of ABP determinants can be targeted by both pathogenic assaults and normal cellular programs, e.g. cell division and epithelial-mesenchymal transition (EMT),[6,39–42] cellular regulation of ABP

appears to be important for tissue integrity. Several factors including those regulating cell viability and proliferation may bias one side in this 'tug of war' between optimal (wild type) cells and sub-optimal *scrib* KD cells. Besides the proper distribution of ABP determinants, their amount may be important for optimal cells to defend against premalignant cells' loss of ABP. Because recent study suggests that Scrib levels by themselves serve as a means of regulating tissue growth,[36] quantitative regulation of Scrib may play a role in balancing between tissue growth and homeostasis.

In summary, this study reveals a unique mechanism in regulating epithelial growth and homeostasis. Our findings open the horizon of cellular mechanisms of ABP through communications among optimal and sub-optimal cells. Further studies will be needed for understanding global ABP maintenance and its relevance in diseases.

Limitations of the study

Although our data reveal that ABP restoration serves as a unique mechanism supporting tissue homeostasis, precise molecular mechanisms behind this remain to be determined. Further study is needed to understand how the cells expressing full length Scrib (optimal cells) affect ABP of neighboring sub-optimal cells.

STAR★METHODS

Detailed methods are provided in the online version of this paper and include the following:

- KEY RESOURCES TABLE
- RESOURCE AVAILABILITY
  - Lead contact
  - Materials availability
  - Data and code availability
- EXPERIMENTAL MODEL AND SUBJECT DETAILS
- METHOD DETAILS
  - DNA constructs
  - Transgenic flies
  - Cell culture and Co-immunoprecipitation
  - Immunostaining and *in situ* hybridization
  - Imaging and image analysis
- QUANTIFICATION AND STATISTICAL ANALYSIS

SUPPLEMENTAL INFORMATION

Supplemental information can be found online at https://doi.org/10.1016/j.isci.2023.106490.

ACKNOWLEDGMENTS

We are grateful to Martti Montanari, Tamsin Samuels and Tambet Tõnissoo for thoughtful comments on the manuscript. We thank the Light Microscopy Unit and Electron Microscopy Unit of the Institute of Biotechnology, University of Helsinki for their support. *Drosophila* work was supported by the Hi-Fly core facility, funded by Helsinki Institute of Life Science and Biocenter Finland. We thank D. Bilder, G. Halder, and C. Doe for fly stocks and antibodies. This work was supported by grant 347569 from the Academy of Finland, the Sigrid Jusélius Foundation to O.S., and the Center of Excellence in Experimental and Computational Developmental Biology from the Academy of Finland to O.S. and M.M.

AUTHOR CONTRIBUTIONS

Conceptualization, Y.H., J.G., and O.S.; Methodology, Y.H., J.G., and O.S.; Investigation, Y.H. and J.G.; Formal analysis, Y.H., J.G., and O.S.; Resources, S-M.M. and M.M.; Writing – Original Draft, Y.H., J.G., and O.S.; Review and Editing, Y.H., J.G., and O.S.; Funding Acquisition, M.L.M. and O.S.; Supervision, O.S.

DECLARATION OF INTERESTS

The authors declare no competing interests.

Received: December 20, 2021
Revised: February 27, 2023
Accepted: March 18, 2023
Published: March 22, 2023

REFERENCES

1. Bilder, D. (2004). Epithelial polarity and proliferation control: links from the Drosophila neoplastic tumor suppressors. Genes Dev. *18*, 1909–1925. https://doi.org/10.1101/gad.1211604.

2. Hariharan, I.K. (2015). Organ size control: lessons from Drosophila. Dev. Cell *34*, 255–265. https://doi.org/10.1016/j.devcel.2015.07.012.

3. Thompson, B.J. (2013). Cell polarity: models and mechanisms from yeast, worms and flies. Development *140*, 13–21. https://doi.org/10.1242/dev.083634.

4. Campanale, J.P., Sun, T.Y., and Montell, D.J. (2017). Development and dynamics of cell polarity at a glance. J. Cell Sci. *130*, 1201–1207. https://doi.org/10.1242/jcs.188599.

5. Lang, C.F., and Munro, E. (2017). The PAR proteins: from molecular circuits to dynamic self-stabilizing cell polarity. Development *144*, 3405–3416. https://doi.org/10.1242/dev.139063.

6. Bonello, T.T., and Peifer, M. (2019). Scribble: a master scaffold in polarity, adhesion, synaptogenesis, and proliferation. J. Cell Biol. *218*, 742–756. https://doi.org/10.1083/jcb.201810103.

7. Schulte, J., Charish, K., Que, J., Ravn, S., MacKinnon, C., and Auld, V.J. (2006). Gliotactin and Discs large form a protein complex at the tricellular junction of polarized epithelial cells in Drosophila. J. Cell Sci. *119*, 4391–4401. https://doi.org/10.1242/jcs.03208.

8. Zeitler, J., Hsu, C.P., Dionne, H., and Bilder, D. (2004). Domains controlling cell polarity and proliferation in the Drosophila tumor suppressor Scribble. J. Cell Biol. *167*, 1137–1146. https://doi.org/10.1083/jcb.200407158.

9. Stephens, R., Lim, K., Portela, M., Kvansakul, M., Humbert, P.O., and Richardson, H.E. (2018). The scribble cell polarity module in the regulation of cell signaling in tissue development and tumorigenesis. J. Mol. Biol. *430*, 3585–3612. https://doi.org/10.1016/j.jmb.2018.01.011.

10. Yang, C.C., Graves, H.K., Moya, I.M., Tao, C., Hamaratoglu, F., Gladden, A.B., and Halder, G. (2015). Differential regulation of the Hippo pathway by adherens junctions and apical-basal cell polarity modules. Proc. Natl. Acad. Sci. USA *112*, 1785–1790. https://doi.org/10.1073/pnas.1420850112.

11. Cordenonsi, M., Zanconato, F., Azzolin, L., Forcato, M., Rosato, A., Frasson, C., Inui, M., Montagner, M., Parenti, A.R., Poletti, A., et al. (2011). The Hippo transducer TAZ confers cancer stem cell-related traits on breast cancer cells. Cell *147*, 759–772. https://doi.org/10.1016/j.cell.2011.09.048.

12. Hansen, C.G., Moroishi, T., and Guan, K.L. (2015). YAP and TAZ: a nexus for Hippo signaling and beyond. Trends Cell Biol. *25*, 499–513. https://doi.org/10.1016/j.tcb.2015.05.002.

13. Huang, J., Wu, S., Barrera, J., Matthews, K., and Pan, D. (2005). The Hippo signaling pathway coordinately regulates cell proliferation and apoptosis by inactivating Yorkie, the Drosophila Homolog of YAP. Cell *122*, 421–434. https://doi.org/10.1016/j.cell.2005.06.007.

14. Gaspar, P., and Tapon, N. (2014). Sensing the local environment: actin architecture and Hippo signalling. Curr. Opin. Cell Biol. *31*, 74–83. https://doi.org/10.1016/j.ceb.2014.09.003.

15. Dupont, S., Morsut, L., Aragona, M., Enzo, E., Giulitti, S., Cordenonsi, M., Zanconato, F., Le Digabel, J., Forcato, M., Bicciato, S., et al. (2011). Role of YAP/TAZ in mechanotransduction. Nature *474*, 179–183. https://doi.org/10.1038/nature10137.

16. Fernández, B.G., Gaspar, P., Brás-Pereira, C., Jezowska, B., Rebelo, S.R., and Janody, F. (2011). Actin-Capping Protein and the Hippo pathway regulate F-actin and tissue growth in Drosophila. Development *138*, 2337–2346. https://doi.org/10.1242/dev.063545.

17. Sansores-Garcia, L., Bossuyt, W., Wada, K.I., Yonemura, S., Tao, C., Sasaki, H., and Halder, G. (2011). Modulating F-actin organization induces organ growth by affecting the Hippo pathway. EMBO J. *30*, 2325–2335. https://doi.org/10.1038/emboj.2011.157.

18. Justice, R.W., Zilian, O., Woods, D.F., Noll, M., and Bryant, P.J. (1995). The Drosophila tumor suppressor gene warts encodes a homolog of human myotonic dystrophy kinase and is required for the control of cell shape and proliferation. Genes Dev. *9*, 534–546. https://doi.org/10.1101/gad.9.5.534.

19. Davis, J.R., and Tapon, N. (2019). Hippo signalling during development. Development *146*. https://doi.org/10.1242/dev.167106.

20. Sun, S., and Irvine, K.D. (2016). Cellular organization and cytoskeletal regulation of the Hippo signaling network. Trends Cell Biol. *26*, 694–704. https://doi.org/10.1016/j.tcb.2016.05.003.

21. Rübsam, M., Mertz, A.F., Kubo, A., Marg, S., Jüngst, C., Goranci-Buzhala, G., Schauss, A.C., Horsley, V., Dufresne, E.R., Moser, M., et al. (2017). E-cadherin integrates mechanotransduction and EGFR signaling to control junctional tissue polarization and tight junction positioning. Nat. Commun. *8*, 1250. https://doi.org/10.1038/s41467-017-01170-7.

22. Takeichi, M. (2014). Dynamic contacts: rearranging adherens junctions to drive epithelial remodelling. Nat. Rev. Mol. Cell Biol. *15*, 397–410. https://doi.org/10.1038/nrm3802.

23. Tepass, U., and Hartenstein, V. (1994). The development of cellular junctions in the Drosophila embryo. Dev. Biol. *161*, 563–596. https://doi.org/10.1006/dbio.1994.1054.

24. Harden, N., Wang, S.J.H., and Krieger, C. (2016). Making the connection - shared molecular machinery and evolutionary links underlie the formation and plasticity of occluding junctions and synapses. J. Cell Sci. *129*, 3067–3076. https://doi.org/10.1242/jcs.186627.

25. Lane, N.J., and Swales, L.S. (1982). Stages in the assembly of pleated and smooth septate junctions in developing insect embryos. J. Cell Sci. *56*, 245–262.

26. Izumi, Y., and Furuse, M. (2014). Molecular organization and function of invertebrate occluding junctions. Semin. Cell Dev. Biol. *36*, 186–193. https://doi.org/10.1016/j.semcdb.2014.09.009.

27. Chen, C.L., Schroeder, M.C., Kango-Singh, M., Tao, C., and Halder, G. (2012). Tumor suppression by cell competition through regulation of the Hippo pathway. Proc. Natl. Acad. Sci. USA *109*, 484–489. https://doi.org/10.1073/pnas.1113882109.

28. Kanda, H., and Igaki, T. (2020). Mechanism of tumor-suppressive cell competition in flies. Cancer Sci. *111*, 3409–3415. https://doi.org/10.1111/cas.14575.

29. Khoury, M.J., and Bilder, D. (2020). Distinct activities of Scrib module proteins organize epithelial polarity. Proc. Natl. Acad. Sci. USA *117*, 11531–11540. https://doi.org/10.1073/pnas.1918462117.

30. Ma, X., Shao, Y., Zheng, H., Li, M., Li, W., and Xue, L. (2013). Src42A modulates tumor invasion and cell death via Ben/dUev1a-mediated JNK activation in Drosophila. Cell Death Dis. *4*, e864. https://doi.org/10.1038/cddis.2013.392.

31. Pinheiro, D., and Bellaïche, Y. (2018). Mechanical force-driven adherens junction remodeling and epithelial dynamics. Dev. Cell *47*, 3–19. https://doi.org/10.1016/j.devcel.2018.09.014.

32. Buszczak, M., Paterno, S., Lighthouse, D., Bachman, J., Planck, J., Owen, S., Skora, A.D., Nystul, T.G., Ohlstein, B., Allen, A., et al. (2007). The carnegie protein trap library: a versatile tool for Drosophila developmental

studies. Genetics *175*, 1505–1531. https://doi.org/10.1534/genetics.106.065961.

33. Rice, C., De, O., Alhadyian, H., Hall, S., and Ward, R.E. (2021). Expanding the junction: new insights into non-occluding roles for septate junction proteins during development. J. Dev. Biol. *9*, 11. https://doi.org/10.3390/jdb9010011.

34. Lee, T., and Luo, L. (1999). Mosaic analysis with a repressible cell marker for studies of gene function in neuronal morphogenesis. Neuron *22*, 451–461.

35. Pan, Y., Alegot, H., Rauskolb, C., and Irvine, K.D. (2018). The dynamics of hippo signaling during drosophila wing development. Development *145*. https://doi.org/10.1242/dev.165712.

36. Huang, Y., Gui, J., Myllymäki, S.M., Roy, K., Tõnissoo, T., Mikkola, M.L., and Shimmi, O. (2022). Scribble and α-Catenin cooperatively regulate epithelial homeostasis and growth. Front. Cell Dev. Biol. *10*, 912001. https://doi.org/10.3389/fcell.2022.912001.

37. Baker, N.E. (2020). Emerging mechanisms of cell competition. Nat. Rev. Genet. *21*, 683–697. https://doi.org/10.1038/s41576-020-0262-8.

38. Bowling, S., Lawlor, K., and Rodríguez, T.A. (2019). Cell competition: the winners and losers of fitness selection. Development *146*. https://doi.org/10.1242/dev.167486.

39. Varga, J., and Greten, F.R. (2017). Cell plasticity in epithelial homeostasis and tumorigenesis. Nat. Cell Biol. *19*, 1133–1141. https://doi.org/10.1038/ncb3611.

40. Javier, R.T., and Rice, A.P. (2011). Emerging theme: cellular PDZ proteins as common targets of pathogenic viruses. J. Virol. *85*, 11544–11556. https://doi.org/10.1128/JVI.05410-11.

41. Javier, R.T. (2008). Cell polarity proteins: common targets for tumorigenic human viruses. Oncogene *27*, 7031–7046. https://doi.org/10.1038/onc.2008.352.

42. Yamben, I.F., Rachel, R.A., Shatadal, S., Copeland, N.G., Jenkins, N.A., Warming, S., and Griep, A.E. (2013). Scrib is required for epithelial cell identity and prevents epithelial to mesenchymal transition in the mouse. Dev. Biol. *384*, 41–52. https://doi.org/10.1016/j.ydbio.2013.09.027.

43. Gui, J., Huang, Y., and Shimmi, O. (2016). Scribbled optimizes BMP signaling through its receptor internalization to the Rab5 endosome and promote robust epithelial morphogenesis. PLoS Genet. *12*, e1006424. https://doi.org/10.1371/journal.pgen.1006424.

44. Bischof, J., Maeda, R.K., Hediger, M., Karch, F., and Basler, K. (2007). An optimized transgenesis system for Drosophila using germ-line-specific phiC31 integrases. Proc. Natl. Acad. Sci. USA *104*, 3312–3317. https://doi.org/10.1073/pnas.0611511104.

STAR★METHODS

KEY RESOURCES TABLE

REAGENT or RESOURCE	SOURCE	IDENTIFIER
Antibodies		
Mouse anti-β-Galactosidase	Promega	Cat# Z378A; RRID:AB_2313752
Rabbit anti-Scrib	C. Doe	N/A
Mouse anti-Dlg	DSHB	Cat# 4F3; RRID:AB_528203
Rat anti-DE-Cad	DSHB	Cat# DCAD2; RRID:AB_528120
Rat anti-α-Cat	DSHB	Cat# DCAT-1; RRID: AB_532377
Mouse anti-β-Cat	DSHB	Cat# N2 7A1 ARMADILLO; RRID:AB_528089
Mouse anti-Coracle	DSHB	Cat# C566.9; RRID:AB_1161642
Mouse anti-Coracle	DSHB	Cat# C615.16; RRID:AB_1161644
Rabbit anti-MYC	Santa Cruz Biotechnology	Cat# sc-789; RRID:AB_631274
Rabbit anti-aPKC	Santa Cruz Biotechnology	Cat# sc-937; RRID:AB_632229
Mouse anti-MYC	Cell Signaling Technology	Cat# 2276; RRID:AB_331783
Rabbit anti-cleaved-Dcp-1	Cell Signaling Technology	Cat# 9578; RRID:AB_2721060
Mouse anti-GFP	Millipore	Cat# MAB3580; RRID:AB_94936
Mouse anti-γ-tubulin	Sigma-Aldrich	Cat# T5326; RRID:AB_532292
Goat anti-mouse IgG Alexa 488	Thermo Fisher Scientific	Cat# A-11001; RRID:AB_2534069
Goat anti-mouse IgG Alexa 568	Thermo Fisher Scientific	Cat# A-11004; RRID:AB_2534072
Goat anti-mouse IgG Alexa 647	Thermo Fisher Scientific	Cat# A-21236; RRID:AB_2535805
Goat anti-rabbit IgG Alexa 568	Thermo Fisher Scientific	Cat# A-11011; RRID:AB_143157
Goat anti-rabbit IgG Alexa 647	Thermo Fisher Scientific	Cat# A-21244; RRID:AB_2535812
Goat anti-rat IgG Alexa 488	Thermo Fisher Scientific	Cat# A-11006; RRID:AB_141373
IRDye 680RD goat anti-mouse	LI-COR	RRID AB_2651128
IRDye 800CW goat anti-rabbit	LI-COR	RRID AB_2651127
Chemicals, peptides, and recombinant proteins		
Blue protein standard	NEB	Cat# P7706
GeneRuler DNA ladder	Thermo Fisher Scientific	Cat# SM0332
FuGENE HD transfection reagent	Promega	Cat# E2311
DAPI	Sigma-Aldrich	Cat# D9542;
Alexa 488 phalloidin	Thermo Fisher Scientific	Cat# A12379
Formaldehyde	Sigma-Aldrich	Cat# 252549
Critical commercial assays		
GFP-Trap® Agarose	Chromo Tek	Cat# sta-100
Experimental models: Cell lines		
Drosophila S2 cells	*Drosophila* genomics resource center	Cell line #S2-DGRC

(*Continued on next page*)

Continued

REAGENT or RESOURCE	SOURCE	IDENTIFIER
Experimental models: Organisms/strains		
D. melanogaster: UAS-mCherry RNAi	Bloomington *Drosophila* Stock Center	RRID:BDSC_35785
D. melanogaster: UAS-wts:MYC	Bloomington *Drosophila* Stock Center	RRID:BDSC_44250
D. melanogaster: UAS-wts RNAi	Bloomington *Drosophila* Stock Center	RRID:BDSC_34064
D. melanogaster: ex-lacZ	Bloomington *Drosophila* Stock Center	RRID:BDSC_44248
D. melanogaster: nub-GAL4	Bloomington *Drosophila* Stock Center	RRID:BDSC_25754
D. melanogaster: apterous-GAL4	Bloomington *Drosophila* Stock Center	RRID:BDSC_3041
D. melanogaster: UAS-scrib RNAi	Bloomington *Drosophila* Stock Center	RRID:BDSC_35748
D. melanogaster: scrib^{2}	Bloomington *Drosophila* Stock Center	RRID:BDSC_41775
D. melanogaster: UAS-NrxIV RNAi	Bloomington *Drosophila* Stock Center	RRID:BDSC_39071
D. melanogaster: UAS-GFP RNAi	Bloomington *Drosophila* Stock Center	RRID:BDSC_44415
D. melanogaster: UAS-yki.168A.V5	Bloomington *Drosophila* Stock Center	RRID:BDSC_28818
D. melanogaster: UAS-yki.V5	Bloomington *Drosophila* Stock Center	RRID:BDSC_28819
D. melanogaster: UAS-bsk.DN	Bloomington Drosophila Stock Center	RRID:BDSC_6409
D. melanogaster: tubP-GAL80^{ts}	Bloomington *Drosophila* Stock Center	RRID:BDSC_7017
D. melanogaster: UAS-kune RNAi	Vienna *Drosophila* Resource Center	RRID:_ V108224
D. melanogaster: UAS-shg/DE-cad RNAi	Vienna *Drosophila* Resource Center	RRID:_V8024
D. melanogaster: Scrib:GFP	(Buszczak et al., 2007)	RRID:_CA07683
D. melanogaster: FRT82B-scrib^{5}	D. Bilder	N/A
D. melanogaster: ex-lacZ, ptc-GAL4, UAS-EGFP	G. Halder	N/A
D. melanogaster: UAS-scrib^{FL}*:MYC*	Gui et al., 2016[43]	N/A
D. melanogaster: UAS-scrib^{LRR}*:MYC*	Gui et al., 2016[43]	N/A
D. melanogaster: UAS-scrib^{dLRR}*:MYC*	Gui et al., 2016[43]	N/A
D. melanogaster: UAS-α-Cat:MYC	This study	N/A
D. melanogaster: UAS- scrib^{LRR}*-α-Cat:MYC*	This study	N/A
D. melanogaster: UAS-kune:MYC	This study	N/A
D. melanogaster: UAS-kune-α-Cat:MYC	This study	N/A
D. melanogaster: UAS-DE-cad^{FL}*:MYC*	This study	N/A
D. melanogaster: UAS-DE-cad^{dCyt}*-α-Cat:MYC*	This study	N/A
D. melanogaster: yw; ubi-scrib:EGFP	This study	N/A
Recombinant DNA		
pUASt.attB	(Bischof et al., 2007)[44]	N/A
scrib cDNA	Addgene	#42064
Oligonucleotides		
α-Cat sense-T3: 5′GCAATTAACCCTCAC TAAAGGCGATTTCGGACAGATA GCTTTGAAATG-3′	Merck	N/A
α-Cat anti-sense-T7: 5′TAATACGACTCACTATAGGGTAATAC TTTCCAGACGCTCTTCGAGCA-3′	Merck	N/A
Software and algorithms		
ImageJ/Fiji	http://fiji.sc/	N/A
ZEN Microscope software	https://www.zeiss.com/microscopy/int/products/microscope-software.html	N/A

(*Continued on next page*)

Continued

REAGENT or RESOURCE	SOURCE	IDENTIFIER
LAS X Microscope software	https://www.leica-microsystems.com/products/microscope-software/p/leica-las-x-ls/downloads/	N/A
Other		
Zeiss LSM700	Zeiss	N/A
Leica SP8	Leica	N/A
Leica DM6000B	Leica	N/A
Odyssey Infrared Imaging System	LI-COR	N/A

RESOURCE AVAILABILITY

Lead contact

Further information and requests for resources and reagents should be directed to and will be fulfilled by the lead contact, Osamu Shimmi (osamu.shimmi@helsinki.fi).

Materials availability

All reagents used in this study will be made available on request to the lead contact.

Data and code availability

- Additional details about the microscopy images reported in this paper is available from the lead contact upon request.
- This paper does not report original code.
- Any additional information required to reanalyze the data reported in this paper is available from the lead contact upon request.

EXPERIMENTAL MODEL AND SUBJECT DETAILS

D. melanogaster strains were raised at 25°C unless otherwise mentioned. To induce MARCM clones, larvae were heat-shocked for 2 h at 37°C at 72 h after egg laying (AEL), followed by wing imaginal disc collection two days after heat shock.

Larvae for conditional knockdown mediated by *ptc-GAL4* and *nub-GAL4* were raised at 21°C for 3 days before transferred to 29°C and 27°C, respectively, followed by wing imaginal disc collection on the date indicated.

METHOD DETAILS

DNA constructs

All coding sequences (CDS) were amplified through PCR, tagged with MYC or GFP at the C-terminus and cloned into the pUASt.attB.[44] The constructs encoding the Scrib fragments were generated previously.[43] α-Cat was cloned into BglII and KpnI, Kune into KpnI and XbaI, and DE-Cad into NotI and KpnI sites of pUASt.attB, respectively. The chimeric constructs were generated by inserting α-Cat CDS into the C-terminus of Scrib^{LRR}, Kune or DE-Cad (lacking the cytosolic domain, aa1-1348) before the stop codon.

Transgenic flies

The plasmids for transgenesis were constructed as described above. Transgenic fly stocks were generated by injecting the plasmids into yw; (PBac y[+]-attP VK00018) embryos by BestGene Inc.

Cell culture and Co-immunoprecipitation

Drosophila S2 cells were used to produce recombinant proteins for immunoprecipitation (IP) and Western blotting (WB). The plasmids containing indicated CDS and *tubP-GAL4* were co-transfected into the cells using FuGENE HD transfection reagent according to the manufacturer's protocol, followed by cell harvest

and lysis in IP lysis buffer (25 mM Tris-HCl pH 7.4, 150 mM NaCl, 1% NP-40, 1 mM EDTA, 5% glycerol) 3 days after transfection. Cell lysates were subjected to WB and IP using the GFP-Trap Agarose following the manufacturer's protocol. WB was performed probing with the following antibodies: primary antibodies, anti-GFP, and anti-Myc tag; secondary antibodies, anti-mouse IRDye 680 and anti-rabbit IRDye 800. The blots were measured by an Odyssey Infrared Imaging System. All biochemical data shown are representative of three independent assays. The following primary antibodies were used: mouse anti-GFP (1: 5000), mouse anti-γ-tubulin (1:5000), rabbit anti-MYC tag (1:1000).

Immunostaining and *in situ* hybridization

Immunostaining and in situ hybridization were performed following standard procedures. Larvae were fixed in 3.7% formaldehyde at room temperature (RT) for 20 min, then wing imaginal discs were dissected. Samples were then washed 3 × 10 min in PBT, permeabilized for 15 min with PBT, and blocked for 1 h with 5% normal goat serum in PBT at RT. For Immunostaining, incubate with primary antibody was performed at 4°C overnight, then washed 3 times for 10 min in PBT at RT. Secondary antibody incubation was performed for 2 h at RT. The following primary antibodies were used: rabbit anti-Scrib (1:200), mouse anti-Dlg (1:50), rat anti-DE-Cad (1:50), rat anti-α-Cat (1:50), mouse anti-β-Cat (1:50), rabbit anti-MYC tag (1:100), rabbit anti-aPKC (1:100), mouse anti-β-Galactosidase (1:500), mouse anti-MYC tag (1:200), rabbit anti-Dcp-1 (1:200). All secondary antibodies were diluted at 1:200. Digoxigenin-labelled probes for α-Cat RNA were used for *in situ* hybridization and visualized with alkaline phosphatase precipitates.

Imaging and image analysis

Fluorescent images were obtained with a Zeiss LSM700 upright or Leica SP8 upright confocal microscopy, *in situ* hybridization images were obtained with a Leica DM6000B microscopy.

All images were processed and analyzed using ImageJ/FIJI (NIH, https://imagej.nih.gov/ij/). The images presented were composites of stacks (maximum intensity projection) unless otherwise specified. Only linear methods were applied. To measure the Scrib-negative area outside the GFP or MYC-positive domain in the wing pouch, the region was manually outlined and measured using the selection tools in ImageJ/FIJI. For the measurement of relative intensity of Scrib, DE-Cad, α-Cat, β-Cat and Scrib:GFP, a 20 μm × 100 μm area of ptc-GAL4 apical domain (~6 micron-thickness) was selected and subjected to intensity calculation using ImageJ/FIJI. Obtained values were subsequently standardized to that of the abutting posterior region.

QUANTIFICATION AND STATISTICAL ANALYSIS

Statistical analyses were performed using GraphPad Prism software (v.9.0.2, GraphPad). The number for all quantified data is indicated in the figure legends. Data are means ±95% confidence intervals (CIs). Statistical significance was calculated by the two tailed t-test method. **** represents ****p< 0.0001.